



Real-time Health Monitoring of Mechanical Structures

Eric Keller and Asok Ray*

*Mechanical Engineering Department, The Pennsylvania State University,
University Park, PA 16802, USA*

The paper presents development and experimental validation of a real-time health monitoring and nondestructive evaluation (NDE) method for residual life prediction of ductile-alloy structures. Application areas include fatigue crack damage in mechanical structures such as those in aircraft, surface ship, submarines, civil infrastructures, and power plants. The technical approach relies on fusion of heterogeneous information derived from physics-based models of fatigue damage and real-time sensor data. This ultrasonic-sensor-based NDE method requires theoretical formulation and experimental validation: (i) a stochastic damage model under fatigue crack initiation and propagation; and (ii) filter algorithms for on-line damage estimation and remaining life. The analytical part of the work is supported by laboratory experimentation on a special-purpose fatigue test apparatus that is equipped with computer-based ultrasonic, optical, and mechanical sensing devices.

Keywords fatigue damage · non-destructive evaluation · ultrasonics · real-time sensing

1 Introduction

Complex mechanical systems, such as aircraft, surface ship, submarines, civil infrastructures, and power plants, often have widely varying usage patterns. Due to the difficulty and expense of implementation in complex structures, usage is often measured by quantities such as flight hours for aircraft, years for bridges and roads, and number of starts for diesel engines. It is also assumed that the state of damage in a mechanical structure bears a direct correlation with the amount of usage. However, one structure may be used in a benign manner and another may be used in a manner that causes a drastic reduction of service life. For example, engines are more highly stressed in aircraft that are used for pilot training [4]. This causes difficulty and expense in

maintenance and logistics efforts due to the fact that maintenance actions and operation planning are based on aggregate usage, and thus, as faults and anomalies are experienced over time, premature replacements of parts and periodic maintenance become more frequent to assure safety of the most heavily used structures. A solution of this problem is on-line failure diagnosis and prognosis that allow remaining life prediction for critical structural components of operating machinery under anticipated load profiles.

Due to the nonstationary and random nature of fatigue crack propagation in ductile-alloy structures, it is difficult to determine the current state of damage and remaining service life of machinery components. For structures where failures have grave consequences, current practice is either conservative estimation of service life, or frequent

*Author to whom correspondence should be addressed.
E-mail: axr2@psu.edu

expensive and time-consuming inspections, or both. Real-time sensing of damage would allow on-going re-evaluation and extension of service life and inherent protection against unforeseen early failures. If no inspection or on-line prediction of damage is available, it is prudent to retire or repair the structure when the worst possible crack trajectory reaches some critical length reduced by a (possibly over-conservative) safety margin. This crack trajectory should be determined for an acceptable risk level from the observed statistics; however, this is not commonly done due to the lack of an appropriate stochastic model of crack propagation. There is a need for development of an operational strategy that will extend the service life of mechanical structures while fulfilling the mission objectives. That is, a trade-off must be achieved between the operational performance and service life. The current state of the art attempts to achieve these objectives by inspections and maintenance actions based on fixed usage intervals. On-line sensing of the damage state and prediction of remaining service life will reduce the frequency of inspections and increase the mean time between major maintenance actions on serviceable structures.

This paper presents real-time health monitoring and nondestructive evaluation (NDE) of ductile-alloy structures, which includes sensing and analytical prediction of fatigue crack damage for information-based decision and control. The work reported in this paper has been demonstrated on a laboratory-scale test apparatus on specimens having relatively simple geometries so that the underlying concept of real-time health monitoring and NDE can be unambiguously explained from experimental observations. Nevertheless, there are still ample opportunities for utilization of the proposed concept on complex mechanical structures such as an airframe. The NDE system demonstrates a novel approach to on-line estimation of crack damage model parameter(s), which significantly reduces the variability inherent in remaining life prediction.

The paper is organized in six sections and an appendix. Section 2 describes the special-purpose laboratory apparatus for validation of the real-time NDE concept. Section 3 presents an overview of damage sensing supported by a

state-space model of fatigue crack damage that is described in the appendix. Section 4 presents the underlying approach for ultrasonic flaw detection. Section 5 develops a stochastic model of remaining life prediction based on the processed fatigue crack data of ultrasonic flaw detection. Section 6 summarizes and concludes the paper with recommendations for future research.

2 Laboratory Apparatus for Fatigue Damage Testing

The special-purpose test apparatus incorporates the major features of a fatigue crack damage monitoring system within a laboratory setting. The software subsystem of the apparatus provides estimates of the current state of fatigue crack damage and predicted residual life as continuous functions of time under anticipated load profiles.

The special-purpose test apparatus is a uniaxial fatigue testing machine under load control or strain control and can be operated at speeds up to 12 Hz; a detailed description of the apparatus and its design specifications is reported by Keller [2]. The apparatus loads the test specimens by a hydraulic cylinder under the regulation of computer-controlled electro-hydraulic servovalves. The feedback signals are generated from either a load cell or an extensometer and are processed by signal conditioners that include standard amplifiers and signal processing units. The damage estimation and life prediction subsystem consists of damage analysis software and the associated computer hardware. The software subsystem receives real-time data from the heterogeneous measurement devices and operational data from the fatigue testing component of the test apparatus.

The measurement devices for the NDE system consists of the following four types of sensors that are combined for information fusion to reduce the effects of measurement noise and uncertainties at different stages of fatigue crack growth.

- *Long Distance Traveling Optical Microscope:* The Questar QM100 Step Zoom Long distance microscope is the primary instrument for crack length measurement. This microscope is

mounted on a 3-axis stepper motor driven precision stage. The microscope resolves images on the order of 2 microns (μm) at a distance of 15–35 mm.

- *Ultrasonic Flaw Detection:* A piezo-electric transducer is used to inject the acoustic waves into the specimen and a transducer is spatially installed across the crack plane to measure the signal whose signature is attenuated as a function of the crack length.

The process instrumentation and control system for the test apparatus is described below:

- *Closed Loop Servo-hydraulic Test System:* The computer-controlled uniaxial fatigue test system includes a load cell, actuator, hydraulic system, and controller. The system can provide either random loads or random strains to a specimen for both low-cycle and high-cycle fatigue tests at variable amplitude and frequency.
- *Computers for Data Acquisition, Signal Processing, and Engineering Analysis:* In addition to the computer controlling the load frame, a computer is used for image and signal processing. The ultrasonic flaw detection is performed by a third computer. These laboratory computers are interconnected by a local dedicated network for data acquisition, data communications, and control.

3 Real-time Sensing of Fatigue Crack Damage

In structures made of ductile alloys that are subject to fatigue failures, a large part of the service life is spent in crack initiation and in the presence of very small cracks. The overriding goal of this research is to have knowledge of damage state for as much of the life of the structure as possible, and not simply to know when the life of the structure is used up. Thus, for this work, small crack detection and sizing is of primary importance. There are very few methods for detection of very small cracks or flaws that are of comparable size as the microstructural elements of ductile alloys. There

are even fewer methods that are suitable for installations outside of the laboratory.

Although ultrasonic flaw detectors meet the requirements of real-time damage sensing, their implementation is uncommon on structures in service or possibly has not been done to date. Ultrasonic flaw detectors are commonly used in the aerospace and nuclear power industries to detect flaws in structures, and have been used by many researchers for laboratory crack length measurement [9]. While several other ultrasonic NDE techniques are available for off-line inspection, this paper focuses on real time sensing of fatigue crack damage that requires quantification of material degradation using sensor-based automation.

The experiments on the test apparatus, described in Section 2, were conducted in the laboratory air at room temperature to focus on: (i) detection of the initiation of short cracks (down to $\sim 30 \mu\text{m}$ long); and (ii) quantification of their growth behavior as well as the identification of the role of metallurgical microstructure. All tests were run under block loading, with each block except the last featuring a reduction from the previous load.

The test data were collected during fatigue tests performed on specimens of 7075-T6 aluminum alloy. The specimens were $1/8''$ ($\sim 3 \text{ mm}$) thick and $2''$ ($\sim 50 \text{ mm}$) wide with a $1/16'' \times 5/16''$ ($\sim 1.5 \text{ mm} \times 7.5 \text{ mm}$) slot cut at the center. Since the slot ends were rounded, it is essentially equivalent to a hole and is convenient for monitoring and data collection as the crack growth process continues. Since the ends of the notch were smooth, crack formation did not occur at the same time on both sides of the notch or equally through the thickness of the specimen on a given side of the notch.

Crack lengths were measured using a traveling microscope equipped with a camera. The optical observations and load applications were synchronized so that measurements could be taken while the fatigue machine was running. These data are representative of structures under tension–tension loading. The experimental results were in close agreement with predictions of the state-space model of fatigue crack growth [8], which is described in Appendix.

4 Ultrasonic Flaw Detection

This section presents the measurement techniques and the associated analyses for ultrasonic flaw detection. Two different ultrasonic flaw detectors were used in the experiments on the test apparatus described in Section 2.

The ultrasonic flaw detector functions by emitting high frequency acoustic pulses and measuring the signal after it has propagated through the material being measured. Material features such as the grain boundaries, inclusions, stress state, voids, or cracks along the path of the wave do affect the propagation of the signal. A piezo-electric transducer is used to inject the acoustic waves into the specimen. A transducer or an array of transducers is in position across the crack plane to measure the signal. Any flaw or other discontinuity in material properties along the wave path causes a reflection of energy back towards the wave source, and also distorts the signal as seen by a transducer on the other side of the flaw from the source. Preexisting flaws, such as grain boundaries or inclusions cause attenuation in the signal that should not change significantly over the lifetime of a structure, particularly compared to the attenuation caused by a fatigue crack. As with the propagation of any wave, it is possible that discontinuities in the propagation media will cause additive and destructive interference. Attenuation was chosen rather than reflection to avoid the issues of detecting a small signal in noise [1]. However, the analysis of attenuation poses the problem of small change detection in noisy signals.

A 16-element array was used to capture the ultrasonic pulses after they had passed the plane of the crack. The objective was to collect data for crack modeling as well as to demonstrate the feasibility of damage sensing techniques. Analysis of the experimental results shows that no significant information is lost if only one transducer is used for this purpose. The signals for the initial testing consist of a spike pulse that is modulated by the transducers into a band-limited signal with frequencies from 2 to 4 MHz. The second system uses a gated 15 MHz sine wave signal. These systems are approximately equivalent from the perspectives of this experiment. Both systems

emit a signal for a very short portion of the measurement cycle. The short pulses used in the experiments prevent the development of standing waves in the test specimen.

The ultrasonic measurements presented here were taken asynchronously to the load application on the test specimens. Thus, upon crack formation, only a minority of ultrasonic measurements are collected when the crack is closed. Generally, this phenomenon does not significantly affect the observations until the crack length is large enough to almost fully attenuate the ultrasonic signal. In a cyclic load test in the laboratory environment, the crack is closed only for a small portion of the time. However, in an actual application such as aircraft loading, crack closure is potentially more problematic because loads are applied at a much lower rate than measurements can be taken. Since the far-field stress is required for the damage estimation scheme detailed in the second part of this paper, it would be natural to only record ultrasonic measurements that were taken under loads that exceed the crack opening stress. The crack opening stress is available from the algorithm used in the damage estimator presented in later sections.

The wedges used for the transducers in this test are of a high enough angle that the signal may take multiple paths through the test specimen to reach the pickup transducers. The signal that reaches the transducer is then a characteristic pulse of finite duration that must be processed in order to be correlated to the corresponding crack length.

Figure 1 shows the profile of a rectified ultrasonic signal received on an un-cracked test specimen where the abscissa is the time duration of the pulse and the ordinate is the normalized signal strength. It exhibits the evolution of the ultrasonic signal output as the exciting pulse input is repeatedly applied [3]. This phenomenon represents the effects of different transmission modes through the specimen.

Considering each measurement pulse as a vector, the norm of the vector is a representation of the crack length measurement. Three measurement methods were used to analyze the (rectified) ultrasonic signals: the ℓ_2 norm (i.e., square root of energy); inner product of each

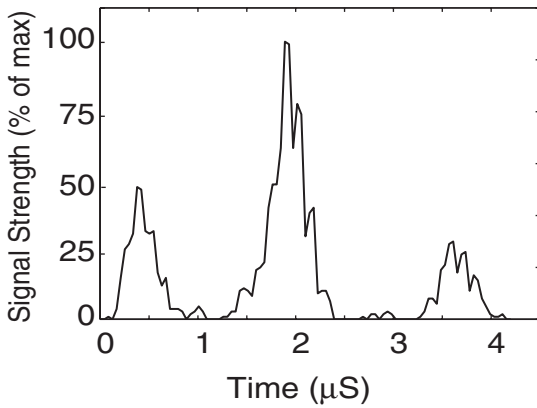


Figure 1 Rectified ultrasonic signal (center-holed 7075-T6 specimen).

signal with a reference signal; and the l_∞ norm (i.e., the peak value).

Computation of an inner product of the signal with a reference signal is largely analogous to having the energy except that it is linearly related to the signal. The major advantage for using the inner product is that the signal emphasizes larger crack lengths to a greater degree than the square root of energy or l_2 norm measurement. For the work presented in the following sections, the peak value or l_∞ norm measurement is also included because it is computationally simplest and matches the microscope crack measurements closely on both left and right sides of crack propagation. All three approaches for attenuation calculation are shown in the two plates of Figure 2 that shows a comparison of ultrasonic signal attenuation and microscope data for crack propagation on both left and right sides of the specimen notch. The attenuation γ is calculated as follows:

$$\gamma = 1 - \frac{\rho[s(t)]}{\rho[s(t_0)]} \quad (1)$$

where $s(t_0)$ is the signal at the initial time t_0 ; $s(t)$ is the signal at the current time t ; and $\rho(\bullet)$ indicates a positive scalar measure (e.g., energy, maximum value, or inner product) of the signal \bullet .

This approach is self-calibrating because the absolute signal level is not used in the crack length analysis. The microscope measurements of crack length in Figure 2 were processed to fit on

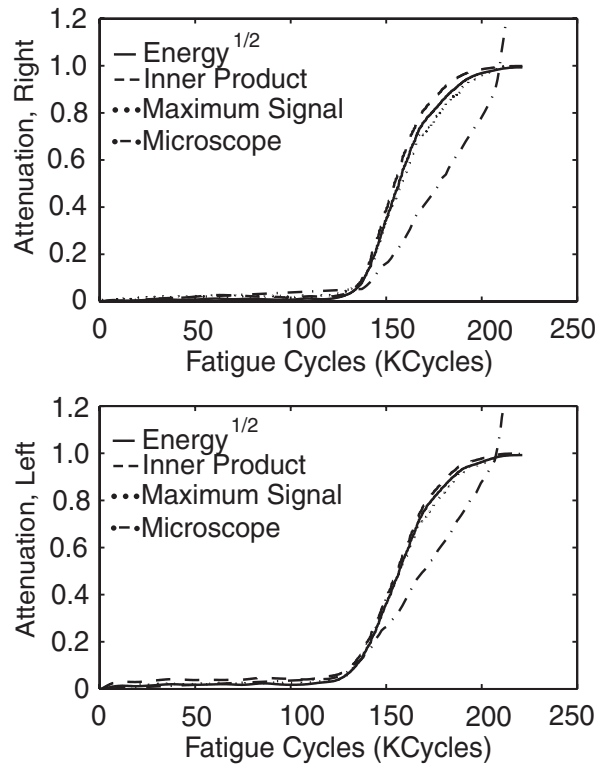


Figure 2 Ultrasonic signal and microscope data (center-holed 7075-T6 specimen).

the same scale as the ultrasonic attenuation by appropriately scaling the crack length from the edge of the notch. The scale factor was chosen so that the average microscope measurement crossed the 100% attenuation line approximately at the same place as the ultrasonic signal reached 100% attenuation. This scaling is not important for the analysis.

Surface cracking was observed within 10,000 cycles from the initiation of testing, but large crack growth was not observed until after 100,000 cycles on most specimens. The specimens were tested with block loading. After cracks had initiated on both sides of the notch, the load was decreased 3 times in blocks of 15,000 cycles each, and then the load was returned to its initial value.

An empirical model has been constructed to calibrate the ultrasonic sensing device for crack length measurements. The calibration curve in Figure 3 exhibits the normalized crack length as a function of the ultrasonic signal attenuation. The data from multiple fatigue crack growth

experiments were aggregated, and a fifth order polynomial fit was generated using least squares fit of the maximum signal value to crack length was found as follows:

$$c_u = c_0 + \sum_{k=0}^5 \alpha_k u^k \quad (2)$$

where u is the ultrasonic signal attenuation, c_u is the ultrasonic measurement of crack length, and c_0 is $\frac{1}{2}$ the notch width. The coefficients of this equation are: $\alpha_0 = 0.019$, $\alpha_1 = 0.861$, $\alpha_2 = -3.16$, $\alpha_3 = 9.372$, $\alpha_4 = -11.655$, $\alpha_5 = 5.57$. Lower order polynomials do not properly capture the desired behavior for small attenuation. The polynomial structure of the calibration curve is not unique as there exist other mathematical forms that might fit the data as well. In particular, it is difficult to fit the sigmoid shape of the attenuation data with the exponential shape of crack growth with a polynomial. Therefore, the orthogonal functions such as Legendre polynomials, or transcendental functions could also be used. This issue should be further investigated to obtain a trade-off between accuracy and computational speed of real-time measurements.

The calibration of the ultrasonic sensing device is in close agreement with the microscope data for a large majority of test specimens for attenuation up to about 80%. It should be noted that an appropriately calibrated ultrasonic instrument is potentially more accurate than optical microscopy in measuring the condition of the specimen because the microscope can only capture the anomaly in grain structure on

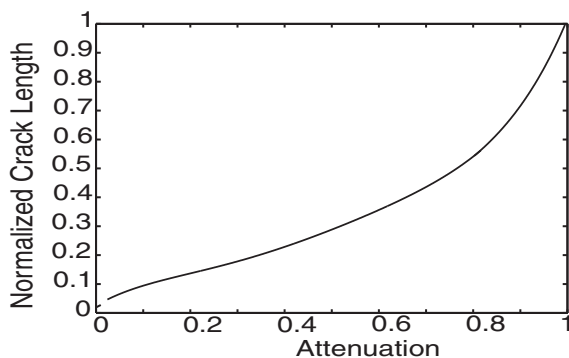


Figure 3 Calibration of crack length to attenuation (center-holed 7075-T6 specimen).

one face of the specimen whereas the ultrasonic measurements are affected by the entire cross section of the crack. This is particularly true when the crack is small, because then the 2-D geometry of the crack may not be well represented by a measurement on the surface. The other consideration while using the microscope is that it is possible for the two sides to have a constant bias in length. It is likely that the accuracy could be improved with better knowledge of crack configuration when the cracks are very small.

5 Damage Parameter Estimation

This section develops a parameter estimator from a stochastic model of remaining life based on the processed crack length data of ultrasonic flaw detection on center-cracked test specimens. As seen in the previous sections, the ultrasonic measurements of crack length are only available for cracks up to a certain length. Thus, it is natural to extrapolate future crack growth with a predictive model, of which many are available. However, due to the random nature of fatigue crack growth, life prediction for an engineered structure is quite difficult, and the available models are only accurate to first order statistics (i.e., in the mean). Since the first order statistics may result in large prediction errors (for example, in the order of 100% or more) for a given crack, it is imperative to mitigate the prediction uncertainties on-line. This is the motivation for the work presented in this section.

Ray [6] and Ray and Patankar [7] have shown that for both constant amplitude cyclic loading without and with overload injection, most of this randomness can be captured by a single (constant) random parameter. Thus, if this result holds for variable amplitude spectrum loading, given an estimator for this parameter, the evolution of future crack growth for a known load profile can be predicted considerably more accurately than that for existing models. The parameter estimation procedure is briefly explained below.

The geometry factor F , is given by: $F = \text{Sec}((\pi/2)(c/w))$ where w is the half width of

the specimen. For $c \ll w$, $F \approx 1$, and this approximation is used in the following analysis to simplify the equations.

Let us normalize the crack length c as: $\theta \equiv c/w$, and the stress range $\Delta S \equiv S^{\max} - S^o$ as $\sigma_t \equiv \Delta S/\Delta S^*$ where ΔS^* is a fixed nominal stress range. Following Ray [6], the governing equation for the stochastic process $\theta_t(\zeta)$ of (normalized) crack growth is obtained as:

$$\delta\theta_t(\zeta) = (\Omega(\zeta) + v_t(\zeta))(\theta_t(\zeta))^{m/2}(\sigma_t)^m \delta t \quad (3)$$

where, ζ indicates a random sample (i.e., test specimen); $\delta\theta_t(\zeta)$ is the (normalized) crack growth increment; t is the current time upon completion a cycle; δt is the increment in number of stress cycles; $\Omega(\zeta)$ is a material-dependent random parameter; v_t is a zero-mean white noise representing variations in the material composition; m is the material-dependent exponent parameter ($2.5 \leq m \leq 5$ for ductile alloys).

Following the rationale provided in previous publications, [6] and [7], $\Omega(\zeta)$ and $v_t(\zeta)$ are statistically independent for all t . A rearrangement of Equation (3) yields:

$$(\theta_t(\zeta))^{-m/2} \delta\theta_t(\zeta) = (\Omega(\zeta) + v_t(\zeta))(\sigma_t)^m \delta t \quad (4)$$

Approximating the above difference equation in the limit as a Riemann Sum, and integrating both sides:

$$\begin{aligned} & \frac{1}{1 - (m/2)} \left(\theta_t(\zeta)^{1-(m/2)} - \theta_{t_0}(\zeta)^{1-(m/2)} \right) \\ & = \Omega(\zeta) \int_{t_0}^t (\sigma_\tau)^m d\tau + \int_{t_0}^t (\sigma_\tau)^m v_\tau(\zeta) d\tau \end{aligned} \quad (5)$$

An incremental measure of damage is defined from time t_0 to time $t \geq t_0$ as:

$$\psi_t(\zeta, t_0) = \frac{1}{1 - (m/2)} \left(\theta_t(\zeta)^{1-(m/2)} - \theta_{t_0}(\zeta)^{1-(m/2)} \right) \quad (6)$$

which is non-negative for $m > 2$ because of non-negative crack growth increment, i.e., $\theta_t(\zeta) \geq \theta_{t_0}(\zeta)$. Note that $\psi_t(\zeta, t) = 0$ for all t . Starting with:

$$\psi_t(\zeta, t_0) = \Omega(\zeta) \int_{t_0}^t (\sigma_\tau)^m d\tau + \int_{t_0}^t (\sigma_\tau)^m v_\tau(\zeta) d\tau \quad (7)$$

the following results are obtained:

$$\begin{aligned} E[\psi_t(\zeta, t_0)] & = E[\Omega(\zeta)] \int_{t_0}^t (\sigma_\tau)^m d\tau \\ \text{Var}[\psi_t(\zeta, t_0)] & = \text{Var} \left[\int_{t_0}^t (\sigma_\tau)^m \Omega(\zeta) d\tau \right] \\ & \quad + \int_{t_0}^t (\sigma_\tau)^{2m} \alpha_\tau d\tau \end{aligned} \quad (8)$$

where α_t is the (time dependent) intensity of the white noise $v_t(\zeta)$ due to variations in the material composition. Based on the constitutive relations reported in Ray [6], we set:

$$E[\Omega] = \mu_\Omega \text{ and } \text{Var}[\Omega(\zeta)(\sigma_\tau)^m] = C \quad (9)$$

A combination of Equations (8) and (9) yields:

$$\begin{aligned} E[\psi_t(\zeta, t_0)] & = \mu_\Omega \int_{t_0}^t (\sigma_\tau)^m d\tau \\ \text{Var}[\psi_t(\zeta, t_0)] & = C(t - t_0)^2 + \int_{t_0}^t (\sigma_\tau)^{2m} \alpha_\tau d\tau \end{aligned} \quad (10)$$

For the constant amplitude case, i.e., $\sigma_t = \sigma$, and homogenous nature of the white noise $v_t(\zeta)$, i.e., $\alpha_t = \alpha$,

$$\begin{aligned} E[\psi_t(\zeta, t_0)] & = \mu_\Omega (\sigma_t)^m (t - t_0) \\ \text{Var}[\psi_t(\zeta, t_0)] & = C(t - t_0)^2 + \sigma^{2m} \alpha (t - t_0) \end{aligned} \quad (11)$$

For sufficiently large t , the term $(t - t_0)^2$ dominates the term $(t - t_0)$ in Equation (11). Therefore, large t , variance in the damage measure is largely determined by the term $C(t - t_0)^2$, which represents the variability captured by the random parameter Ω .

Given the above model of crack growth, a life prediction model is now developed based on the processed crack length data $\{\theta_t\}$ of ultrasonic flaw detection at arbitrary (i.e., nonuniformly spaced) instants of time. The resulting measurement equation is obtained by:

$$y_t(\zeta) \equiv \frac{\theta_t^{1-(m/2)}}{1-(m/2)} + n_t(\zeta) \quad (12)$$

where n_t is a zero-mean stationary white Gaussian noise of known variance representing the noise associated with ultrasonic flaw detection. It follows from Equations (5)–(7) and (12) that

$$\begin{aligned} y_t(\zeta) - y_{t_0}(\zeta) &= \Omega(\zeta) \int_{t_0}^t (\sigma_\tau)^m d\tau \\ &+ \int_{t_0}^t (\sigma_\tau)^m v_\tau(\zeta) d\tau + n_t - n_{t_0} \end{aligned} \quad (13)$$

Let us introduce an auxiliary variable $z_k \equiv y_{t_k} - y_{\tau_{k-1}}$ for any intermediate instant τ_{k-1} such that $t_{k-1} \leq \tau_{k-1} \leq t_k$. Then,

$$\begin{aligned} z_k &= \Omega(\zeta) \int_{\tau_{k-1}}^{t_k} (\sigma_\tau)^m d\tau \\ &+ \int_{\tau_{k-1}}^{t_k} (\sigma_\tau)^m v_\tau(\zeta) d\tau + (n_{t_k} - n_{\tau_{k-1}}) \end{aligned} \quad (14)$$

Considering block loading, i.e., $\sigma_t = \sigma_k$ for all $t_{k-1} < t \leq t_k$, and homogeneous material properties with constant intensity $\alpha_k = \alpha$ of the white noise due to the variations in material composition, yield:

$$\begin{aligned} z_k &= \Omega(\zeta) \sigma_k^m (t_k - \tau_{k-1}) \\ &+ \sigma_k^m \sqrt{\alpha} \beta_{(t_k - \tau_{k-1})}(\zeta) + \varepsilon_k(\zeta) \end{aligned} \quad (15)$$

where $\varepsilon_k(\zeta) \equiv n_{t_k}(\zeta) - n_{\tau_{k-1}}(\zeta)$, with $E[\varepsilon_k] = 0$, and $\text{Var}[\varepsilon_k] = \sigma_n^2 (t_k - \tau_{k-1})$. Defining

$$Z \equiv \begin{bmatrix} z_1 \\ \vdots \\ z_\ell \end{bmatrix}; \quad H \equiv \begin{bmatrix} \sigma_1^m (t_1 - \tau_0) \\ \vdots \\ \sigma_\ell^m (t_\ell - \tau_{\ell-1}) \end{bmatrix}; \quad E \equiv \begin{bmatrix} e_1 \\ \vdots \\ e_\ell \end{bmatrix} \quad (16)$$

where

$$e_k = \sigma_k^m \sqrt{\alpha} \beta_{(t_k - \tau_{k-1})}(\zeta) + \varepsilon_k(\zeta),$$

and thus

$$E[e_k] = 0 \quad \text{and} \quad \text{Var}[e_k] = (\sigma_k^{2m} \alpha + \sigma_n^2) (t_k - \tau_{k-1}) \quad (17)$$

In the matrix notation, Equation (17) yields:

$$Z = H\Omega + E; \quad R = \text{Cov}(E) \quad (18)$$

Then, the weighted least squares estimator of the random parameter Ω based on a batch of data sets is given by:

$$\hat{\Omega} = [H^T R^{-1} H]^{-1} H^T R^{-1} Z \quad (19)$$

We construct a recursive estimator of the random parameter Ω by updating the estimate with each new measurement as it becomes available from the ultrasonic flaw detector. The procedure is delineated below:

$$(H^T R^{-1} H)_\ell^{-1} = \frac{1}{\sum_{k=1}^{\ell} (\sigma_k^{2m} (t_k - \tau_{k-1}) / \sigma_k^{2m} \alpha + \sigma_n^2)} \quad (20)$$

and

$$(H^T R^{-1} Z)_\ell = \sum_{k=1}^{\ell} \left(\frac{\sigma_k^m z_k}{\sigma_k^{2m} \alpha + \sigma_n^2} \right) \quad (21)$$

are both scalar quantities, and thus:

$$\hat{\Omega}_\ell = \frac{(H^T R^{-1} Z)_\ell}{(H^T R^{-1} H)_\ell} \quad (22)$$

after ℓ measurements. Then, the update for a new measurement is given by:

$$\begin{aligned} (H^T R^{-1} Z)_{\ell+1} &= (H^T R^{-1} Z)_\ell + \frac{\sigma_{\ell+1}^m z_{\ell+1}}{\sigma_{\ell+1}^{2m} \alpha + \sigma_n^2} \\ (H^T R^{-1} H)_{\ell+1} &= (H^T R^{-1} H)_\ell + \frac{\sigma_{\ell+1}^{2m} (t_{\ell+1} - \tau_\ell)}{\sigma_{\ell+1}^{2m} \alpha + \sigma_n^2} \end{aligned} \quad (23)$$

The recursive relation for the parameter estimate is:

$$\hat{\Omega}_{\ell+1} = \frac{(H^T R^{-1} Z)_{\ell+1}}{(H^T R^{-1} H)_{\ell+1}} \quad (24)$$

The above recursive relation was implemented and demonstrated with the experimental data for 7075-T6 alloy. Whenever the experiments were not conducted using constant amplitude loading, Equation (24) was updated frequently as the experiments progressed. The data did not necessarily represent center-cracked specimens since the cracks did not always start simultaneously on both sides of the notch. Therefore, the measured crack lengths from both sides were averaged together to generate the data for calculating the parameter estimate $\hat{\Omega}$ in the life prediction model without any noticeable error.

For cycle-by-cycle analysis, the estimator is approximately equivalent to the average of z_k/σ_k^m , and is robust in the sense that the estimated parameter $\hat{\Omega}$ is not sensitive to variations in the noise intensity parameters α and σ_n . Ideally, the noise parameters α and σ_n should be determined a priori. In the absence of prior knowledge of α and σ_n , it is possible to have a rough estimate of these parameters without invoking any significant error. There is a transient period before the estimate reaches the steady state. In practice, starting with a good initial estimate of Ω reduces the settling period of these transients.

Some of the experiments on the test apparatus were conducted with significant changes in load amplitude to observe the effects (e.g., crack retardation) of varying amplitude cyclic stresses on fatigue life. Under these circumstances, the experimental measurements of crack damage increment z_k could be noisy and unpredictable if the measurement interval is small. Therefore, a more accurate estimate of z_k is achieved by combining the ultrasonic sensor data with the state-space model of fatigue crack growth described in the Appendix.

The model of crack growth prediction (see Equation (3) in Section 5 and Equations (A-1)–(A-4) in the Appendix) was tested with repeated estimates of the random parameter Ω ,

made as the experiment progressed, and also by using an averaged estimate $\hat{\Omega}$ of Ω , which is close to the estimate obtained at the point of about 160 fatigue kilocycles. The difference between the results obtained from the models with repeated estimates and a single estimate of Ω were within the bounds of measurement errors of both microscope and ultrasonic observations. This is in agreement with the conclusions of earlier studies (e.g., [5] and [6]) that used a single estimate of the parameter Ω for crack growth prediction over the entire range of fatigue life. Therefore, the prediction model based on a single or a few estimate(s) of Ω is recommended because of computational efficiency and no significant compromise on accuracy.

Figure 4 exhibits a comparison of fatigue crack growth profile of the above predicted model with those obtained from the experimental data of microscope and ultrasonic observations. The experimental data of ultrasonic observations were processed by backward averaging over 8 readings, which is accomplished on-line. These results demonstrate that the estimator can be

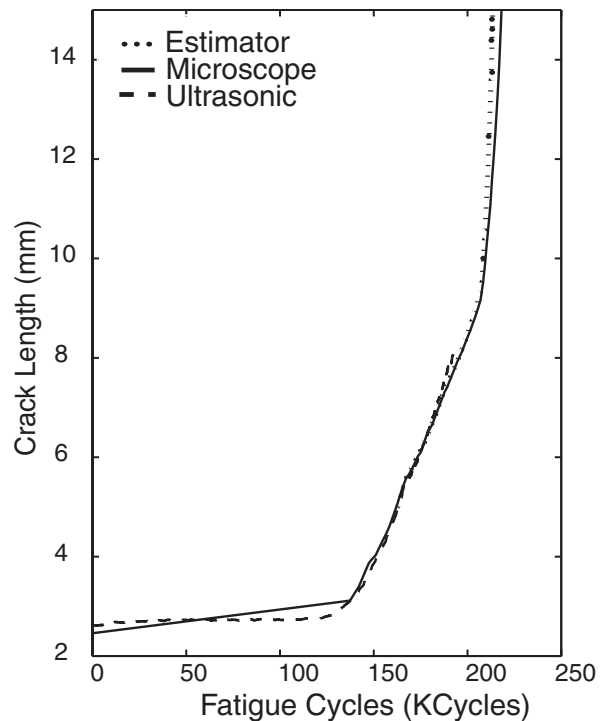


Figure 4 Comparison of crack growth profiles (center-holed 7075-T6 specimen).

used very early in the crack growth process with sufficient accuracy as needed for fatigue crack damage prediction. It is not mandatory to update the estimate of Ω or new crack length measurements frequently.

6 Summary, Conclusions, and Future Research

This paper combines the information contained in ultrasonic measurements of fatigue crack damage with predictions of a state-space model of fatigue crack growth. The predicted model is also validated with the microscope observations that are independent of the ultrasonic data. The goal is to provide a higher fidelity estimate of fatigue crack damage for health monitoring and remaining life prediction than is possible from either method alone.

The ultrasonic sensing system is capable of detecting fatigue crack damage at an early stage and the state-space model captures the effects of crack retardation under variable-amplitude loading by use of the dynamic behavior of the crack opening stress. The life prediction model makes use of a recursive parameter estimator for real-time nondestructive evaluation (NDE) of fatigue crack damage by combining two features: (i) reliable model prediction without the need of storing prolonged load history; and (ii) early damage detection (i.e., in the small crack regime before the onset of widespread damage) using ultrasonic sensor data. This NDE system is able to predict the future progression of fatigue crack damage in a structure with much lower error than a fatigue crack damage model based on typical crack growth parameters. This real-time health monitoring and NDE technique is robust and accurate because ultrasonic measurements of early crack growth are incorporated within the recursive process of damage estimation. The life prediction model can be easily adapted for the large-crack regime by tuning the parameter estimator. However, this is not an important issue because: (i) there are many models available for the large crack regime; (ii) sensors (e.g., strain-based) are available for large crack measurements; and (iii) relatively much less service life is

remaining after the appearance of large cracks (i.e., wide spread fatigue damage is most likely prevalent).

From the perspectives of structural design, health monitoring, and remaining life prediction in mechanical structures, major benefits of the NDE method are envisioned as follows: (i) enhancement of operational safety and reliability due to timely prediction of impending failures; reduction of the life cycle cost by optimization of plant operation; and (ii) maintenance schedule; and augmentation of structural durability and plant availability. Furthermore, the NDE-based health monitoring system reduces the need for services of highly skilled technicians on the work site and can be implemented fleet-wide.

6.1 Recommendations for Future Research

Several areas of future research beyond the work reported in this paper are discussed below:

- Various mechanical structures undergo 2-D fatigue cracks for service life prediction. Therefore, the fatigue damage model presented in this paper need to be extended to 2-D cracks.
- The crack growth model for health monitoring needs to be expanded for different load conditions and geometries. Therefore, the damage parameter estimation technique reported in this paper needs to be extended for additional parameters of crack growth under different crack configurations and different types of loading.
- The paper reports a relatively simple model of ultrasonic signal propagation through a specimen. These results could be further improved from more accurate modeling of ultrasonic waves and their interactions with cracks. In addition, the number of geometries that can be evaluated with this technique are limited to simple holes. Further research is recommended for evaluating this technique with bolted structures and other geometries to widen the number of crack formation sites.

- Although very early stages of fatigue damage (e.g., crack incubation) are difficult to predict and model due to a large number of possible crack configurations, the experimental observations suggest that ultrasonic measurements could be able to discriminate between different crack configurations. Therefore, further experimental research is needed for optically monitoring the notch face as well as the surface of a specimen.
- The experiments reported in this paper are based on 7075-T6 specimens. Although the 7075-T6 alloy is still an important material due to the large installed base, its relatively poor fatigue resistance has led to adoption of over-aged high-strength aluminum alloys. Therefore, further experimental research on advanced materials is recommended.

Acknowledgment

The work was supported by Army Research Office under Grant No. DAAD19-01-1-0646 and National Science Foundation under Grant No. CMS-9819074.

References

1. De Belleval, J.F. and Gherbezza, J.M. (1994). Compensation of ultrasonic transducers response by adapting excitation signals, application to defects evaluation, In: Malague, X.P.V. (ed.), *Advances in signal processing for nondestructive Evaluation of materials*, (pp. 31–42). Kluwer Academic Publishers, Dordrecht, The Netherlands.
2. Keller, E.E. (2001). Real-time sensing of fatigue crack damage for information decision and control, Ph.D. Dissertation, The Pennsylvania State University, May.
3. Langenberg K.J., Fillinger, P., Marklein, R., Zanger, P., Mayer, K. and Kreuttier, T. (1993). Inverse methods and imaging. In: Achenbach, J.D. (ed.), *Evaluation of materials and structures by quantitative ultrasonics*, (pp. 317–398). New York: Springer-Verlag.
4. Mattingly, J.D., Heiser, W.H. and Daley, D.H. (1987). *Aircraft Engine Design*, New York: AIAA, Inc.
5. Newman, J.C. Jr. (1992). *FASTRAN-II — A Fatigue Crack Growth Structural Analysis Program*, NASA Technical Memorandum 104159, Langley Research Center, Hampton, VA.
6. Ray, A. (1999). Stochastic modeling of fatigue crack damage for risk analysis and remaining life prediction. *ASME Journal of Dynamic Systems, Measurements, and Control*, 121(3), 386–393.
7. Ray, A. and Patankar, R. (April–May 1999). A stochastic model of fatigue crack propagation under variable-amplitude loading. *Engineering Fracture Mechanics*, 62(4–5), 477–493.
8. Ray, A. and Patankar, R. (2001). Fatigue crack growth under variable amplitude loading: parts I and II. *Applied Mathematical Modelling*, 25, 979–1013.
9. Resch, M.T. and Nelson, D.V. (1992). An ultrasonic method for measurement of size and opening behaviour of small fatigue cracks. In: Larsen, J.M. and Allison, J.E. (eds.), *Small-Crack Test Methods, ASTM STP 1149*, (pp. 169–196). Philadelphia: ASTM.

APPENDIX

A State-space Model of Fatigue Damage

This appendix presents the relevant part of an analytical model of fatigue crack damage that complements the ultrasonic sensing device presented in the main body of the paper. Ray and Patankar [8] have formulated and validated a state-space model of fatigue crack growth for analysis and synthesis of life-extending controllers. It accounts for the impact of dynamically varying crack opening stress on crack growth rate (e.g., crack retardation and sequence effects) for prediction of structural durability under variable-amplitude loading. The state-space model is an extension of the FASTRAN model [5] that is based on the concept of small cracks in homogeneous materials such as ductile alloys. The FASTRAN model is represented by a nonlinear difference equation in which the crack increment during the k th cycle is obtained as a function of the maximum applied (far-field) stress S_k^{\max} and the crack opening stress S_k^o as:

$$\left. \begin{aligned} \Delta a_k &\equiv a_k - a_{k-1} = h(\Delta K_k^{\text{eff}}) \quad \text{with } h(0) = 0 \\ \Delta K_k^{\text{eff}} &\equiv \sqrt{\pi a_{k-1}} F(a_{k-1}, \tilde{w}) \\ &\times (S_k^{\max} - \max(S_{k-1}^o, S_k^{\min})) \\ &\times U(S_k^{\max} - \max(S_{k-1}^o, S_k^{\min})) \end{aligned} \right\}$$

for $k \geq 1$; $a_0 > 0$

(A-1)

where a_{k-1} and S_{k-1}^o are the crack-length and the crack-opening stress, respectively, during the k th cycle and change to a_k and S_k^o at the expiry of the k th cycle; $F(\bullet, \bullet)$ is a crack-length-dependent correction factor compensating for finite geometry of the specimen with the width parameter \tilde{w} ; the non-negative monotonically increasing function $h(\bullet)$ can be represented either by a closed form algebraic equation: $h(\Delta K_k^{\text{eff}}) = C_1(\Delta K_k^{\text{eff}})^m$ with material constants C_1 and m , or by table lookup [5]; and

$$U(x) = \begin{cases} 0 & \text{if } x < 0 \\ 1 & \text{if } x \geq 0 \end{cases} \quad \text{is the Heaviside function.}$$

We now present the structure of the difference equation that is excited by the cyclic stress input to generate the crack opening stress. To this end, we first consider the steady-state solution of the difference equation under constant amplitude load. This issue has been addressed by several investigators. The steady-state crack-opening stress S_k^{oss} under a constant amplitude cyclic load is a function of the minimum stress S^{min} , the maximum stress S^{max} , the constraint factor α (which is 1 for plane stress and 3 for plane strain), the specimen geometry, and the flow stress S^{flow} (which is the average of the yield strength S^y and the ultimate strength S^{ult}). These relationships are shown to be good for most ductile alloys by Newman [5].

The objective is to construct the difference equation for (non-negative cycle-dependent) crack opening stress S_k^o such that, under different levels of constant-amplitude load, the forcing function S_k^{oss} at the k th cycle matches the crack-opening stress derived from the following empirical relation [5] that is valid for non-zero peak stress (i.e., $S^{\text{max}} \neq 0$) and

$$U(x) = \begin{cases} 0 & \text{if } x < 0 \\ 1 & \text{if } x \geq 0 \end{cases}$$

is the Heaviside function.

We now present the structure of the difference equation that is excited by the cyclic stress input to generate the crack opening stress. To this end, we first consider the steady-state solution of the difference equation under constant

amplitude load. This issue has been addressed by several investigators. The steady-state crack-opening stress S^{oss} under a constant amplitude cyclic load is a function of the minimum stress S^{min} , the maximum stress S^{max} , the constraint factor α (which is 1 for plane stress and 3 for plane strain), the specimen geometry, and the flow stress S^{flow} (which is the average of the yield strength S^y and the ultimate strength S^{ult}). These relationships are shown to be good for most ductile alloys by Newman [5].

The objective is to construct the difference equation for (non-negative and cycle-dependent) crack opening stress S_k^o such that, under different levels of constant-amplitude load, the forcing function S_k^{oss} at the k th cycle matches the crack-opening stress derived from the following empirical relation [5] that is valid for non-zero peak stress (i.e., $S^{\text{max}} \neq 0$):

$$\begin{aligned} S_k^{\text{oss}} &= S^{\text{oss}}(S_k^{\text{max}}, S_k^{\text{min}}, \alpha, F) \\ &= \left(\tilde{A}_k^0 + \tilde{A}_k^1 R_k + \tilde{A}_k^2 (R_k)^2 + \tilde{A}_k^3 (R_k)^3 \right) S_k^{\text{max}} \end{aligned} \quad (\text{A-2})$$

where $R_k \equiv S_k^{\text{min}}/S_k^{\text{max}} U(S_k^{\text{max}})$ for all $k \geq 0$;

$$\begin{aligned} \tilde{A}_k^0 &= (0.825 - 0.34\alpha_k + 0.05(\alpha_k)^2) \\ &\times \left[\cos \left(\frac{\pi S_k^{\text{max}}}{2 S^{\text{flow}}} F(a_{k-1}, \tilde{w}) \right) \right]^{1/\alpha_k} \end{aligned}$$

$$\tilde{A}_k^2 = (1 - \tilde{A}_k^0 + \tilde{A}_k^1 - \tilde{A}_k^3) U(R_k)$$

$$\tilde{A}_k^3 = (2 - \tilde{A}_k^0 + \tilde{A}_k^1 - 1) U(R_k)$$

The constraint factor α_k used above is obtained as a function of the crack length increment Δa_k and α_k represents the state of plane stress or plane strain under which the crack growth is occurring. A procedure for evaluation of α_k is presented in the FASTRAN manual [5]. Since α_k does not significantly change over cycles, it can be approximated as piecewise constant for limited ranges of crack length.

The following constitutive relation, in the form of a nonlinear first order difference equation,

recursively calculates the crack-opening stress S_k^o upon completion of the k th cycle:

$$\begin{aligned}
 S_k^o &= \left(\frac{1}{1+\eta}\right)S_{k-1}^o + \left(\frac{\eta}{1+\eta}\right)S_k^{oss} \\
 &+ \left(\frac{1}{1+\eta}\right)(S_k^{oss} - S_{k-1}^o)U(S_k^{oss} - S_{k-1}^o) \\
 &+ \left(\frac{1}{1+\eta}\right)[S_k^{oss} - S_k^{oss-old}]U(S_{k-1}^{\min} - S_k^{\min}) \\
 &\times [1 - U(S_k^{oss} - S_{k-1}^o)] \quad (A-3)
 \end{aligned}$$

$$\eta = \frac{t S^y}{2 w E} \quad (A-4)$$

where the forcing function S_k^{oss} in the above equation is calculated as if a constant amplitude stress cycle (S_k^{\max}, S_k^{\min}) is applied; similarly, $S_k^{oss-old}$ is given as if a constant amplitude stress cycle (S_k^{\max}, S_k^{\min}) is applied. For constant-amplitude loading, S_k^{oss} is the steady-state solution of S_k^o . In general, the inputs S_k^{oss} and $S_k^{oss-old}$ to Equation (3) are different from the instantaneous crack-opening stress S_k^o under variable-amplitude loading. The Heaviside function $U(S_k^{oss} - S_{k-1}^o)$ in the third term on the right hand side of Equation (3) allows fast rise and slow decay of S_k^o . The last term on the right hand side accounts for the effects of reverse plastic flow. Depletion of the normal plastic zone occurs when the minimum stress S_k^{\min} decreases below its value S_{k-1}^{\min} in the previous cycle, which is incorporated via the Heaviside function $U(S_{k-1}^{\min} - S_k^{\min})$. Note that the overload excitation and reverse plastic flow are mutually exclusive.

The dimensionless parameter η depends on the component thickness t , half-width w , yield strength S^y , and Young's modulus. Following an overload cycle, the duration of crack retardation is controlled by the transients of S_k^o in the state-space model, and hence determined by the stress-independent parameter η in Equation (4). Physically, this duration depends on the ductility of the material that is dependent on many factors including the heat treatment of specimens. Smaller yield strength produces a smaller value of η , resulting in longer duration of the overload effect. Smaller specimen thickness has a similar effect. The crack length a_k and crack opening stress S_k^o are the state variables.

The net effect of a single-cycle overload (i.e., increased S_k^{\max}) is a jump in the effective stress range $\Delta S_k \equiv S_k^{\max} - S_k^o$ resulting in an increase in the crack growth increment in the present cycle. Shortly after the expiration of the overload (i.e., S_k^{\max} returning to the original lower value), S_k^o starts decreasing slowly from its increased value. The result is a decrease in ΔS_k , which causes the crack growth rate to diminish.

Subsequently, after returning to the original constant-amplitude stress, as S_k^o slowly relaxes back to its original state, the crack growth rate resumes the original value. A single overload initially increases crack growth rate for a few cycles and then gradually decreases over a much higher number of cycles until it reaches the original value. The crack growth is therefore retarded due to the fast rise and slow decay of S_k^o .